Article

A Novel Electrochemiluminescence Biosensor based on 3-D DNA Nanomachine Signal Probe Powered by Protein-Aptamer Binding Complex for Ultrasensitive Mucin 1 Detection

Xinya Jiang, Haijun Wang, Huijun Wang, Ying Zhuo, Ruo Yuan, and Yaqin Chai

Anal. Chem., **Just Accepted Manuscript** • DOI: 10.1021/acs.analchem.7b00347 • Publication Date (Web): 10 Mar 2017

A Novel Electrochemiluminescence Biosensor based on 3-D DNA Nanomachine Signal Probe Powered by Protein-Aptamer Binding Complex for Ultrasensitive Mucin 1 Detection

Xinya Jiang, Haijun Wang, Huijun Wang, Ying Zhuo, Ruo Yuan*, Yaqin Chai*

Key Laboratory of Luminescent and Real-Time Analytical Chemistry (Southwest University), Ministry of Education, College of Chemistry and Chemical Engineering, Southwest University, Chongqing 400715, PR of China

* Corresponding author. Tel.: +86-23-68252277; Fax: +86-23-68253172.

E-mail address: yuanruo@swu.edu.cn (R. Yuan), yqchai@swu.edu.cn (Y. Q. Chai)

Abstract:

Herein, we fabricated a novel electrochemiluminescence (ECL) biosensor for ultrasensitive detection of mucin 1 (MUC1) based on a three-dimensional (3-D) DNA nanomachine signal probe powered by protein-aptamer binding complex. The assembly of 3-D DNA nanomachine signal probe achieved the cyclic reuse of target protein based on the protein-aptamer binding complex induced catalyzed hairpin assembly (CHA), which overcame the shortcoming of protein conversion with enzyme cleavage or polymerization in the traditional examination of protein. In addition, $CoFe_2O_4$, a mimic peroxidase, was used as the nanocarrier of the 3-D DNA nanomachine signal probe to catalyze the decomposition of co-reactant H_2O_2 to generate numerous reactive hydroxyl radical $OH^{\cdot}$ as the efficient accelerator of *N*-(aminobutyl)-*N*-(ethylisoluminol) (ABEI) ECL reaction to amplify the luminescence signal. Simultaneously, the assembly of 3-D DNA nanomachine signal probe was executed in solution, which led to abundant luminophore ABEI be immobilized around the $CoFe_2O_4$ surface with amplified ECL signal output since the CHA reaction was occurred unencumberedly in all directions under homogeneous environment. The prepared ECL biosensor showed a favorable linear response for MUC1 detection with a relatively low detection limit of 0.62 fg mL^{-1}. With excellent sensitivity, the strategy may provide an efficient method for clinical application, especially in trace protein determination.

INTRODUCTION

Protein biomarkers, as one important class of biomarkers, can be indicative of disease state according to their high expression or low expression in serum or tissue.[1,2] Due to the prevalence, high rate of recurrence, potential lethality and low protein level in nascent stage of cancer, it is particularly valuable to develop rapid, reliable and sensitive detection strategy for trace protein. Recently, target recycling amplification strategy has attracted increasing interest in highly sensitive detection of biomolecules[3,4] for it can yield an apparent detectable signal even in a trace level of target. In most reported biosensors, the common method to achieve the recycling of target protein is converting protein into output single-stranded DNA through enzyme cleavage or polymerization, which was then used to participate in the fabrication of biosensor.[5-8] Despite the fact that this method can achieve sensitive detection of protein with reliability and specificity at the trace level, it still encounters the drawbacks of time-consuming, high cost, and complexity. Therefore, it is significant to develop a direct protein recycling strategy to overcame the protein conversion in the traditional examination of protein to simplify the operation, shorten the analysis time and facilitate the sensitive protein detection.

Owing to the diversity, predictability and exquisite specificity of DNA hybridization, DNA-based nanomachines such as DNA walks,[9-11] DNA motors[12-14] and DNA tweezers[15,16] have been successfully constructed. However, most DNA nanomachines were performed under one-dimensional (1-D) or two-dimensional (2-D) tracks which restrained the capture of payloads in a certain degree. Recently, a few

DNA nanomachines performed on three-dimensional (3-D) material have been reported. For example, Zhang et al. introduced a new 3-D DNA nanomachine that drived by proteins or nucleic acids.[17] Yang et al. developed an enzyme-powered 3-D DNA nanomachine for DNA walking, payload release and biosensing.[18] These 3-D DNA nanomachines have been demonstrated to represent several advantages over the existent 1-D or 2-D DNA nanomachines due to the high DNA loading density on 3-D material. However, these DNA nanomachines faced the drawback of high cost since they need energy provided by DNAzymes, protein enzymes or chemical fuel to propel nanomachines. Therefore, designing a 3-D DNA nanomachine without enzyme drive is quite essential. Alternatively, catalyzed hairpin assembly (CHA)[19,20] as a robust and ripe nonenzymatic DNA hybridization strategy has attracted increasing interest due to its high efficiency, short analysis time and recycling of the target. Taking advantages of the CHA and 3-D DNA nanomachine, it is desirable to assemble an effective 3-D DNA nanomachine signal probe using nonenzymatic CHA for highly efficient application in biosensing. Furthermore, nanomaterial-based peroxidase mimetics such as Pt,[21] PdIr,[22] Fe_3O_4,[23] V_2O_5[24] *etc*. have been demonstrated to show several advantages (high catalytic activity, high stability, easy storage, low cost) over natural enzymes. $CoFe_2O_4$, a magnetic nanoparticle which is more stable than Fe_3O_4 in air, has been reported to exhibit superior peroxidase-like activity.[25] Therefore, $CoFe_2O_4$ could show great promise in improvement the ECL intensity of N-(aminobutyl)-N-(ethylisoluminol) (ABEI)-H_2O_2 system for it could catalyze the decomposition of H_2O_2 to produce reactive hydroxyl radical $OH^{\cdot}$. In addition,

$CoFe_2O_4$ could also achieve high DNA loading density due to its large surface area and rapid separation. Thus, $CoFe_2O_4$ could be an ideal candidate for the assembly of 3-D DNA nanomachine signal probe.

In the present work, we presented an ultrasensitive ECL biosensor for Mucin 1 (MUC1) detection based on an effective 3-D DNA nanomachine signal probe powered by protein-aptamer binding complex, which overcame the shortcoming of protein conversion with enzyme cleavage or polymerization to achieve the direct protein recycling in the fabrication of biosensor. Briefly, as shown in Scheme 1A, the 3-D $CoFe_2O_4$@Au was firstly functionalized with hairpin1 (HP1) and single-stranded DNA2 (S2) to obtain the 3-D track ($CoFe_2O_4$@Au-S2-HP1) for CHA reaction. In the presence of target MUC1, the aptamer hairpin structure could be opened to form a MUC1-aptamer binding complex (abbreviated as MUC1-A) with an exposed DNA segment as the catalyst of CHA reaction. For the reason that the exposed DNA segment within the aptamer hairpin could interact with a toehold on HP1. As a consequence, the $CoFe_2O_4$@Au-S2-HP1-MUC1-A was obtained with a new exposed DNA segment within HP1, which could hybridize to a toehold on ABEI modified hairpin2 (ABEI-HP2) and then induce branch migration to form a tripartite complex of $CoFe_2O_4$@Au-S2-HP1-MUC1-A-ABEI-HP2. Ultimately, via the strand displacement process, the tripartite complex reformed into the most thermodynamically steady state of $CoFe_2O_4$@Au-S2-HP1-ABEI-HP2 (3-D DNA nanomachine signal probe) with the release of the CHA catalyst MUC1-A. The released MUC1-A further participated in the subsequent reaction cycles, achieving the

target recycling as well as leading to abundant ABEI be immobilized on the surface of $CoFe_2O_4$. The ECL biosensor based on the proposed 3-D DNA nanomachine signal probe activated by protein-aptamer binding complex exhibited a convenient, efficient and sensitive detection for MUC1 with a detection limit down to femtomole. In addition, this strategy could be readily expanded to detect other biomolecules sensitively, especially provided a novel avenue for trace protein detection in nascent stage of cancer.

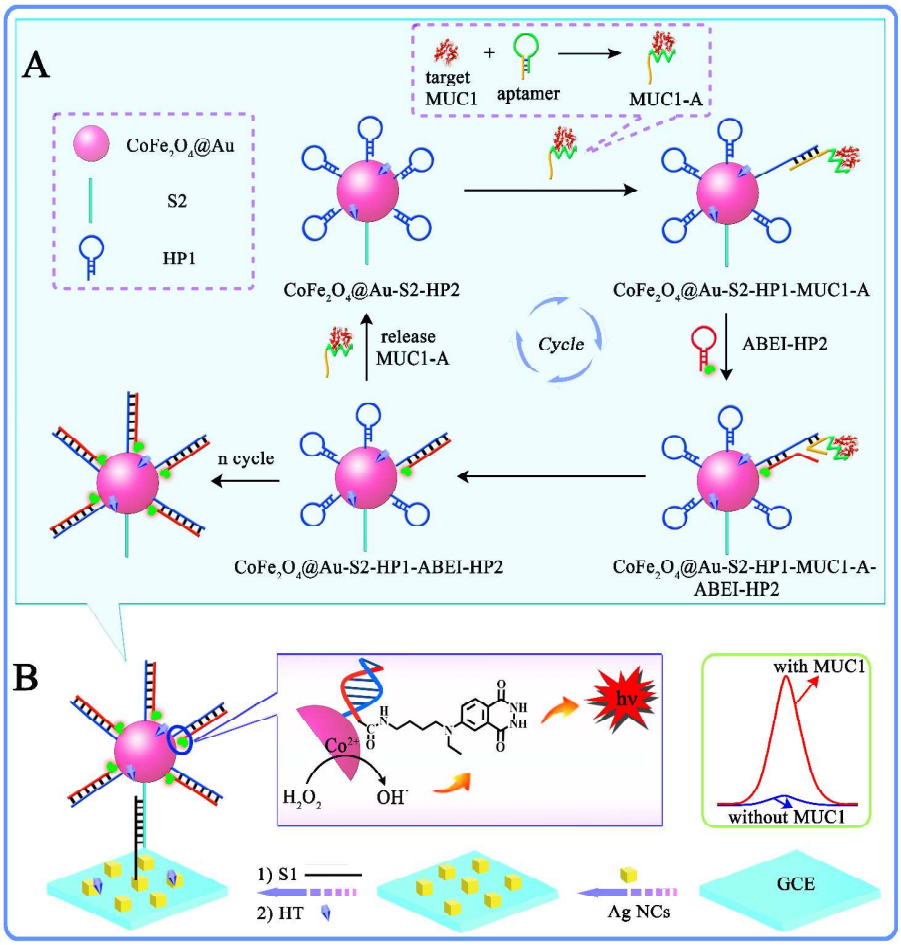

Scheme 1. (A) The assembly process of 3-D DNA nanomachine signal probe induced by protein-aptamer binding complex. (B) Schematic diagrams of the construction and the luminescence reaction mechanism of the biosensor.

EXPERIMENTAL SECTION

Reagents and materials. 1-ethyl-3-[3-dimethylaminopropyl] carbodiimide hydrochloride (EDC), hexanethiol (HT), *N*-(4-aminobutyl)-*N*-ethylisoluminol (ABEI), and N-hydroxysuccinimide (NHS) were obtained from Sigma-Aldrich Co. (St. Louis, MO, USA). Ethylene glycol, sodium citrate, polyvinylpyrrolidone (PVP), $FeCl_3 \cdot 6H_2O$, $HAuCl_4 \cdot 4H_2O$, $Co(NO_3)_2 \cdot 6H_2O$, NaOH, $AgNO_3$ and H_2O_2 were purchased from Chemical Reagent Co. (Chongqin, China). Lysine, [3-(2-aminoethyl)aminopropyl] dimethoxysilane (AAPDMS) was purchased from J&K Scientific Ltd. (Beijing, China). Mucin 1 (MUC1) ELISA Kit was purchased from North Connaught Biotechnology Co. Ltd. (Shanghai, China). DNA oligonucleotides (see Table 1) utilized in the study were synthesized and purified by Sangon Inc. (Shanghai, China). In addition, the involved buffers were showed as follows. DNA store buffer (pH 8.0): 1×TE buffer (10 mM Tris-HCl, 1.0 mM EDTA). DNA hybridization buffer (pH 7.4): 10 mM Tris-HCl, 1.0 mM EDTA and 1.0 M $MgCl_2$. The detection phosphate buffer (PBS, pH 8.0): 0.1 M Na_2HPO_4, 0.1 M KH_2PO_4 and 0.1 M KCl. Ultrapure water was used throughout this experimental process.

Table 1. The list of all DNA oligonucleotide sequences used in our experiment.

Name	Oligonucleotide sequences (from 3' to 5')
HP1	HS-CGTTCCAGTCGACCTATGAGCACACCGGTCCCATAGGTCGACT
HP2	CCTATGAGCACCCTATGGGACCGGTGTGCTCATAGGTCGACT-COOH
S1	GAAATATAGTAGACCGGTCGCGCTAGGCCGATCCTTCCTCCCGTCTC-NH_2
S2	GAAGACGGGAGGAAGGATCGGCCTAGCGCGACCGGTCTACTATATTTC-SH
Aptamer	GGTCCCATAGGTTTCCTAGTTGACGAGTCGACCTATGGGACCGGTGTGCT

Instruments. In the whole detection process, a conventional three-electrode system which contains platinum wire, Ag/AgCl electrode and modified glassy carbon electrode was utilized to accomplish the ECL experiments. For ECL and electrochemical impedance spectroscopy (EIS) experiments, an MPI-A ECL analyzer (Xi'an Remax Electronics, China) and a CHI 660C electrochemical workstation (Shanghai Chenhua Instruments, China) were used respectively. The morphologies of the materials were characterized by scanning electron microscopy (SEM, S-4800). For revealing the compositions of the materials, an X-ray photoelectron spectroscopy (XPS, Thermoelectricity Instruments, U.S.A.) and a UV-vis spectrophotometer (UV-2450, Shimadzu, Japan) were utilized. A DYCP-31E electrophoretic device (WoDeLife Sciences Instrument Co., Ltd., China) was used to perform the gel electrophoresis experiment.

Synthesis of Ag nanocubes (Ag NCs). The Ag NCs was synthesized in a typical method on the basis of a previous literature[26] with little modification. Concretely, 5 mL of ethylene glycol was firstly heated for 1 h at 160 ^{o}C. Then, 3 mL of $AgNO_3$ solution (0.3 M) and 3 mL of PVP (0.45 M) dissolved in ethylene glycol respectively were added to the above hot ethylene glycol solution. Subsequently, the reaction was let to react for 40 min under 160 ^{o}C with stirring. Finally, after thorough washing and centrifugation for three times, the obtained Ag NCs was then dispersed into ultrapure water for further use.

Synthesis of $CoFe_2O_4$@Au-S2-HP1 magnetic nanomaterial. Firstly, the $CoFe_2O_4$ magnetic nanomaterial was synthesized according to the literature.[27] The obtained

$CoFe_2O_4$ was dried in the vacuum oven at 70 ^oC for 10 hours after sufficient washing and centrifugation. Then, the $CoFe_2O_4$@Au magnetic nanomaterial was synthesized using an in-situ reduction method. Briefly, amino groups were firstly introduced on the surface of $CoFe_2O_4$ (1 mg mL^{-1}) by adding 40 μL of AAPDMS with gentle shaking for over night. After magnetic separation, the obtained NH_2-functionalized $CoFe_2O_4$ was dispersed in 1 mL of ultrapure water and 1 mL of $HAuCl_4$ (1%) with stirring for 30 min. Subsequently, 1 mL of sodium citrate (1%) was added and reacted for 6 h under gentle shaking. Thus, the $CoFe_2O_4$@Au magnetic nanomaterial was obtained via magnetic separation and then redispersed in 1 mL of ultrapure water. Finally, S2 (200 μL, 2.5 μM) and HP1 (400 μL, 2.5 μM) were added into the 1 mL of $CoFe_2O_4$@Au solution and allowed to react for 14 h at room temperature. Unreacted reagents were separated via magnetic separation after blocking the nonspecific binding sites with 1 mM HT for 2 h. The $CoFe_2O_4$@AuNPs-S2-HP1 magnetic nanomaterial was separated from solvents by magnetic separation for two times and redispersed in ultrapure water for further use.

Synthesis of ABEI-HP2. ECL luminescent reagent ABEI labeled HP2 (ABEI-HP2) was synthesized using EDC and NHS as the crosslinking agent by the following steps. First, the carboxyl groups of HP2 (100 μL, 5 μM) were activiated for 2 h using EDC (30 μL, 0.2 M) and NHS (30 μL, 0.05 M). Then, 40 μL of ABEI (0.02 M) was added into the above mixture solution and reacted for over night. Thus, the ABEI-HP2 signal probes were synthesized.

Assembly of 3-D DNA nanomachine signal probe. Prior to use, the aptamer

oligonucleotide was firstly denatured at 95°C for 5 min to form a hairpin structure. As depicted in Scheme 1A, the target MUC1 was firstly mixed with aptamer to form different concentrations of MUC1-A binding complex as the catalyst of the CHA reaction. Then, a total volume of 50 μL of the MUC1-A complex with different concentration and 50 μL of ABEI-AP2 were added into 100 μL of $CoFe_2O_4$@AuNPs-S2-HP1 magnetic nanomaterial solution. Followed by incubation for 2 h, the 3-D DNA nanomachine signal probe of $CoFe_2O_4$@AuNPs-S2-HP1-HP2-ABEI was formed. After removing the unreacted reagents by magnetic separation, the obtained $CoFe_2O_4$@AuNPs-S2-HP1-HP2-ABEI signal probe was redispersed in 100 μL of Tri-HCl containing Mg^{2+} for further use.

Fabrication of the ECL biosensor. As shown in Scheme 1B, 5 μL of the Ag NCs suspension was firstly cast onto the cleaned GCE surface which was burnished with 0.3 μm and 0.5 μm alumina powder successively. After dried at room temperature, 10 μL of S1 (2.5 μM) was dripped on the Ag NCs modified electrode surface and incubated at 4 °C for 16 h. Then, the electrode surface was blocked with HT (1 mM) for 2 h after thorough washing with ultrapure water. Following that, 10 μL of the obtained 3-D DNA nanomachine signal probe $CoFe_2O_4$@AuNPs-S2-HP1-HP2-ABEI was dropped onto the S1 and Ag NCs modified electrode surface and incubated for 2 h at 37 °C. Ultimately, the obtained ECL aptasensor was placed in 2 mL PBS (pH 8.0, 2 mM H_2O_2) and conducted with an MPI-A ECL analyzer (0.2-0.6V, 100 mV s^{-1}).

RESULTS AND DISCUSSION

Characterization of different materials. The morphology and dimension of Ag

nanocrystal and $CoFe_2O_4$ magnetic nanomaterial were characterized with scanning electron microscopy (SEM), as shown in Figure 1A and 1B. In Figure 1A, the Ag nanocrystal exhibited a typical nanocube structure with a mean edge length of about 200 nm and a smooth surface. Furthermore, the corners and the edges of AgNCs were slightly truncated. In addition, Figure 1B presented that the $CoFe_2O_4$ magnetic nanomaterial had a spherical structure with a good uniformity and an average dimension of about 55 nm. However, the surface of $CoFe_2O_4$ was extremely rough, indicating that $CoFe_2O_4$ may has a relatively more active site for the decomposition of H_2O_2.

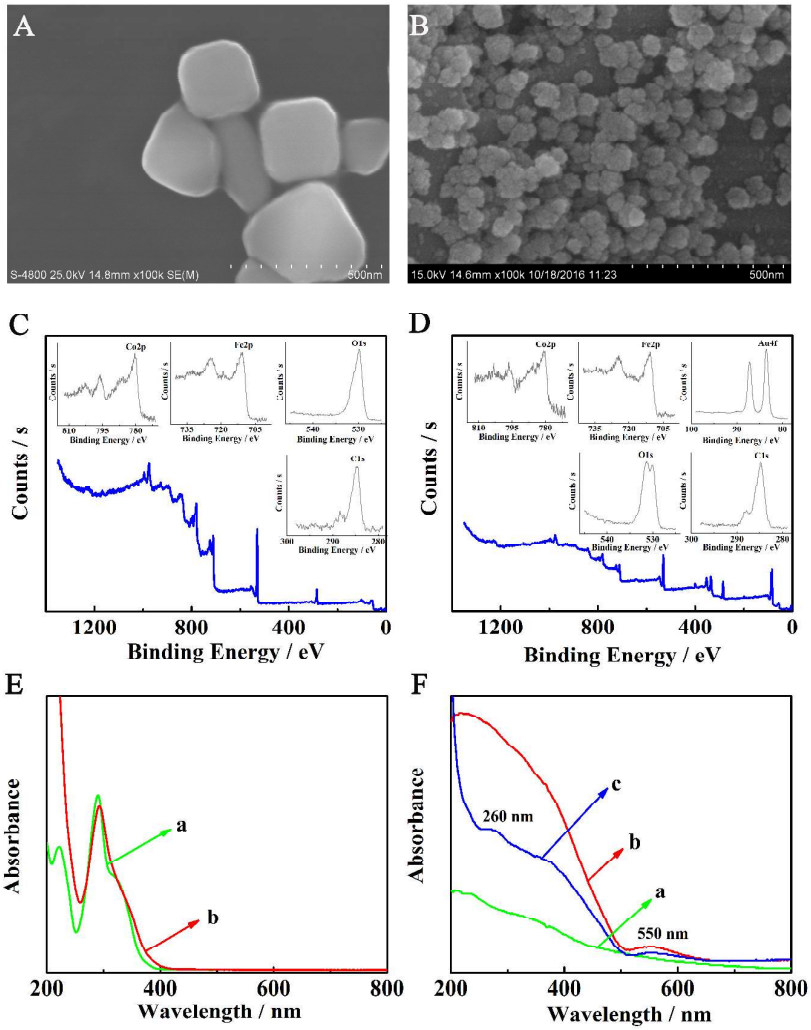

Figure 1. SEM of AgNCs (A) and $CoFe_2O_4$ (B). XPS analysis about the wide scan survey spectra of $CoFe_2O_4$ (C) and $CoFe_2O_4$@Au (D). (E) UVs of ABEI (a) and ABEI-HP2 (b) and (F) UVs of $CoFe_2O_4$ (a), $CoFe_2O_4$@Au (b) and $CoFe_2O_4$@Au-HP1-S2 (c).

The detailed information about the element composition of $CoFe_2O_4$ and $CoFe_2O_4$@Au were characterized with X-ray photoelectron spectroscopy (XPS), as showed in Figure 1C and 1D. Figure 1C revealed the wide scan survey spectra of $CoFe_2O_4$, the Co2p, Fe2p, O1s and C1s peaks were observed respectively at 780.5 eV, 710.9 eV, 529.9 eV and 284.7 eV. Compared with $CoFe_2O_4$, the wide scan survey spectra of $CoFe_2O_4$@Au (Figure 1D) revealed the presence of Au4f peak at 83.55 eV besides Co2p, Fe2p, O1s and C1s, indicating that Au nanoparticles were successfully in-situ reduced on the $CoFe_2O_4$ surface. In addition, the concentrations of these elements on $CoFe_2O_4$ and $CoFe_2O_4$@Au surface were summarized in Table 2.

Table 2. Elemental surface analysis of $CoFe_2O_4$ and $CoFe_2O_4$@Au conducted by XPS.

Samples	Co / %	Fe / %	O / %	C / %	Au / %
$CoFe_2O_4$	13.53	19.29	43.56	23.61	0
$CoFe_2O_4$@Au	5.44	8.27	35.89	44.84	5.55

Moreover, UV-vis absorption spectra were performed to confirm the successful synthesis of ABEI-HP2 and 3-D $CoFe_2O_4$@Au-S2-HP1 track. As showed in Figure 1E, ABEI exhibited two characteristic absorbance peaks at 222 nm and 289 nm (curve a). However, the ABEI-HP2 displayed only one characteristic absorbance peak at 292

nm (Figure 1E, curve b) with a disappearance peak at 222 nm. The reason could be ascribed to the consumption of amino group during the reaction between ABEI and HP2, indicating the successful modification of ABEI on HP2. In addition, compared the UV-vis absorption spectra of $CoFe_2O_4$ (Figure 1F, curve a), the $CoFe_2O_4$@Au displayed an absorption peak at 550 nm (Figure 1F, curve b) indicating the successful assembly of AuNPs on $CoFe_2O_4$. Furthermore, after HP1 and S2 loading on $CoFe_2O_4$@Au, a new absorption peak occurred at 260 nm (Figure 1F, curve c) which corresponded to the typical DNA absorption. All these results demonstrated the successful synthesis of 3-D $CoFe_2O_4$@Au-S2-HP1 track.

Feasibility investigation. Polyacrylamide gel electrophoresis (PAGE, 16%) was applied to verify the feasibility of CHA reaction triggered by protein-aptamer binding complex. As outlined in Figure 2A, HP1, HP2 and aptamer exhibited a single band, respectively (lane-a, b, c). As expected, the HP1, HP2 and aptamer did not hybridize to each other (lane-d vs a, b, c) for the complementary regions were embedded within the hairpin stems. However, an apparently new band with slower mobility was appeared (lane-e) in the presence of target MUC1, indicating the successful formation of double-stranded nucleic acid of H1-H2. The reason was ascribed to that MUC1 could open the aptamer hairpin structure to expose a ssDNA region within aptamer as the catalyst of CHA which could then hybridize to a toehold on HP1. The newly exposed ssDNA region within HP1 further hybridized to a toehold on HP2 and triggered branch migration to form the most thermodynamically favourable configuration of H1-H2.

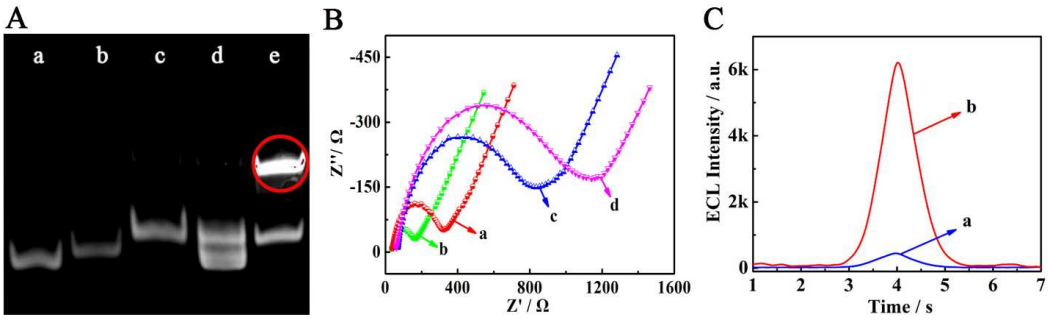

Figure 2. (A) PAGE analysis for CHA reaction. lane-a: HP1; lane-b: HP2; lane-c: aptamer; lane-d: HP1+HP2+aptamer; lane-e: HP1+HP2+aptamer+MUC1. (B) EIS characterization of each modified electrode: (a) bare GCE, (b) AgNCs/GCE, (c) S1/AgNCs/GCE (d) HT/S1/AgNCs/GCE. Working buffer: 5 mM $[Fe(CN)_6]^{4-/3-}$ containing 0.1 M KCl. (C) ECL characterization: (a) without target MUC1, (b) with target MUC1 (1 ng mL^{-1}). Working buffer: 0.1 M PBS (pH 8.0) containing 2 mM H_2O_2.

Next, the feasibility of the proposed biosensor was further confirmed by EIS and ECL measurements. Figure 2B showed the Nyquist plot of the impedance curves obtained from different modified electrodes. The Nyquist plot obtained from bare electrode had a small semicircle (curve a), suggesting a low electron-transfer resistance. After immobilization of Ag NCs on the bare electrode, the semicircle of Nyquist plot decreased a bit (curve b). However, a significant semicircle curve appeared (curve c) when DNA S1 was assembled on electrode surface, indicating that S1 was successfully immobilized on electrode surface and then impeded the transmission of electron. The semicircle curve further increased after using HT to block the nonspecific binding for the formed molecule layer blocked the electron transfer. Therefore, these results indicated that the sensing interface was demonstrated

to be successfully fabricated.

Figure 2C showed the ECL intensity of the proposed biosensor in the absence and presence of target MUC1. In the absence of MUC1, a low ECL signal was obtained (curve a). However, a significant ECL signal appeared (curve b) in the presence of MUC1 (1 ng mL^{-1}), indicating the successful immobilization of ECL luminophore on 3-D $CoFe_2O_4$@Au-HP1-S2 track as well as the feasible construction of the biosensor for MUC1 determination.

Detection conditions optimization. The assembly conditions (in solution or on the modified electrode surface) of the 3-D DNA nanomachine signal probe were investigated to obtain a highly efficient signal probe. As showed in Figure 3A, the 3-D DNA nanomachine signal probe obtained on the modified electrode surface exhibited a lower ECL signal (curve a). However, a higher ECL signal was received from the 3-D DNA nanomachine signal probe obtained in solution (curve b). The reason may be attributed to that protein-aptamer binding complex induced CHA reaction could perform unencumberedly in all directions in solution, resulting in large payloads of ECL luminophore (ABEI-HP2) be immobilized on $CoFe_2O_4$ surface. However, the CHA reaction may be impeded by the electrode surface, leading to relatively low payloads of ABEI-HP2. In conclusion, the assembly process occurred in solution could obtain a highly efficient 3-D DNA nanomachine signal probe.

In this study, the reaction time of CHA caused great effect on the loading number of ECL luminophore. Thus, the optimum reaction time of CHA was investigated under 100 fg mL^{-1} target MUC1. Figure 3B revealed the ECL signals corresponding

to different time periods. The ECL signal increased gradually between 0.5 and 2 h and reached a relatively stable value at 2 h. Therefore, 2 h was selected as the optimum reaction time of CHA to shorten the fabrication time and improve the sensitivity of the proposed biosensor.

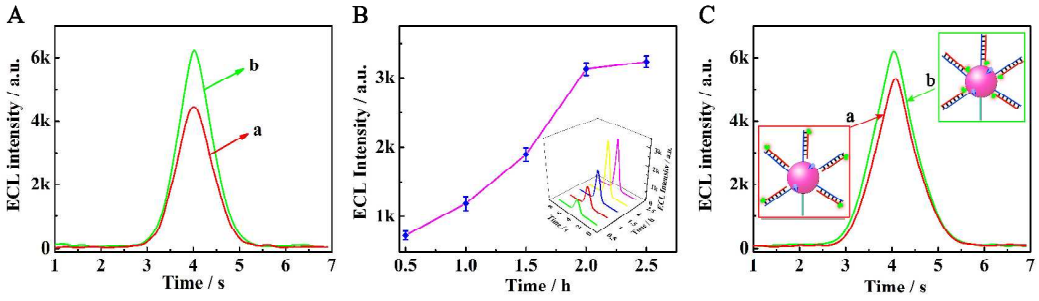

Figure 3. (A) The investigation of the assembly conditions of the 3-D DNA nanomachine signal probe: (a) on the electrode surface, (b) in solution. (B) The optimum reaction time of CHA on the $CoFe_2O_4$@AuNPs surface in the presence of MUC1 (100 fg mL^{-1}). (C) The effect of distance between $CoFe_2O_4$ and ABEI on ECL intensity: (a) ABEI was away from the $CoFe_2O_4$ surface, (b) ABEI was close to the $CoFe_2O_4$ surface.

Moreover, the effect of the distance between the $CoFe_2O_4$ and ABEI on the ECL intensity was also investigated as $CoFe_2O_4$ could catalyst the decomposition of co-reactant H_2O_2 to produce reactive hydroxyl radical $OH^{\cdot}$ which further amplified the ECL signal of ABEI. In this comparative experiment, luminescent reagent ABEI was modified on the two ends of HP2, respectively. Thus, there were two cases when ABEI was further immobilized on the surface of $CoFe_2O_4$: (a) ABEI was away from the $CoFe_2O_4$ surface, (b) ABEI was close to the $CoFe_2O_4$ surface. As showed in Figure 3C, when ABEI was away from the surface of $CoFe_2O_4$, the obtained ECL

intensity (curve a) was lower than the ECL intensity obtained from ABEI was close to the $CoFe_2O_4$ surface (curve b). The results indicated that such a short distance between ABEI and $CoFe_2O_4$ could amplify the ECL intensity due to a relatively shorter electron transfer distance. Therefore, the ABEI was designed to close to the $CoFe_2O_4$ surface when synthesizing the 3-D DNA nanomachine signal probe in this experiment.

Calibration curve for MUC1 detection. Under the optimal experimental conditions, target MUC1 was used to evaluate the quantitative performance of the proposed biosensor. As showed in Figure 4, the ECL signals were recorded with different concentrations of MUC1. Figure 4A clearly exhibited that the ECL signal increased gradually in the concentration range from 1 fg mL^{-1} to 1 ng mL^{-1}. In addition, the ECL intensity can act as a function of the logarithm of MUC1 concentration (Figure 4B). The linear regression equation can be expressed as follows: $I_{ECL} = 6427.3 + 756.3 \lg c$ with the regression coefficient is 0.9984 (curve a). The detection limit was calculated to be 0.62 fg mL^{-1} according to $3S_B/m$ in which the S_B is the standard deviation of the blank sample and m is the slope of the obtained regression equation. For comparison, we fabricated another biosensor that the 3-D DNA nanomachine signal probe was assembled on electrode surface to detect MUC1. The corresponding linear regression equation was showed in Figure 4B (curve b), demonstrating that our proposed biosensor had a higher sensitivity and wider detection range. Furthermore, the proposed biosensor also exhibited a wider detection range and lower detection limit for MUC1 detection compared with other existing methods (Table 3). The reason may

be ascribed to the efficient 3-D DNA nanomachine signal probe, target recycling as well as the excellent catalytic property of $CoFe_2O_4$.

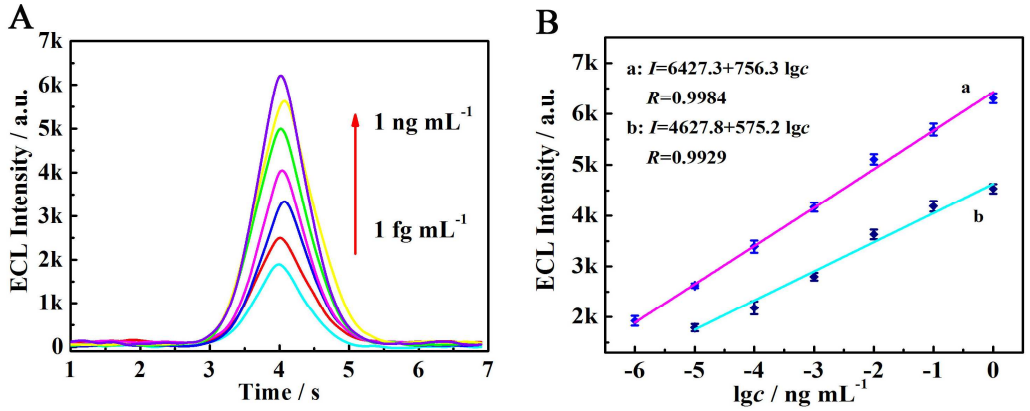

Figure 4. (A) ECL responses of the proposed biosensor on different concentrations (1 fg mL^{-1} to 1 ng mL^{-1}) of MUC1. (B) Calibration plot for MUC1 detection: the 3-D DNA nanomachine signal probe was assembled in solution (a) or on electrode surface (b).

Table 3. Reported methods for MUC1 determination.

Method	Detection range	Detection limit	References
Fluorescence	0.8-39.7 μM	75 μg mL^{-1} (250 nM)	28
Electrochemical	1 nM-1 μM	2.48 μg mL^{-1} (0.827 nM)	29
Electrochemiluminescence	10 fg mL^{-1}-10 ng mL^{-1}	2.80 fg mL^{-1}	30
Electrochemiluminescence	1 fg mL^{-1}-1 ng mL^{-1}	0.62 fg mL^{-1}	This work

Performance of the ECL biosensor. Some important performances, such as selectivity, stability and reproducibility of this proposed biosensor were investigated. As depicted in Figure 5A, ECL intensities obtained from four different concentrations of target MUC1 had a relatively stable signal. The relative standard deviations (RSD) from low cencentration to high concentration were 1.2 %, 2.1 %, 1.3 % and 1.7 %, respectively, indicating an excellent stability of the biosensor. Furthermore, three

other interfering agents such as carcinoembryonic antigen (CEA, obtained from Biocell Company), α-1-fetoprotein (AFP, obtained from Biocell Company) and human Laminin (LN, obtained from Shanghai HuaYi Bio-echnology Co. LTD) were examined respectively by the biosensor to assess its selectivity. As described in Figure 5B, the presence of target MUC1 resulted in a significant increase in ECL intensity than the blank solution (absence of target MUC1). However, the ECL intensities of CEA, AFP and LN were increased insignificantly even their concentrations were 100 times higher than target MUC1. The comparison illustrated an excellent selectivity of the proposed biosensor. For the reproducibility, five of the proposed biosensors with 1 pg mL^{-1} MUC1 prepared in same batch were examined under the same experimental conditions. A semblable ECL signal was received with the RSD of 3.6 %, implying an acceptable reproducibility for determination of MUC1. As a consequence, the proposed biosensor possessed excellent stability, selectivity and reproducibility for MUC1 assay.

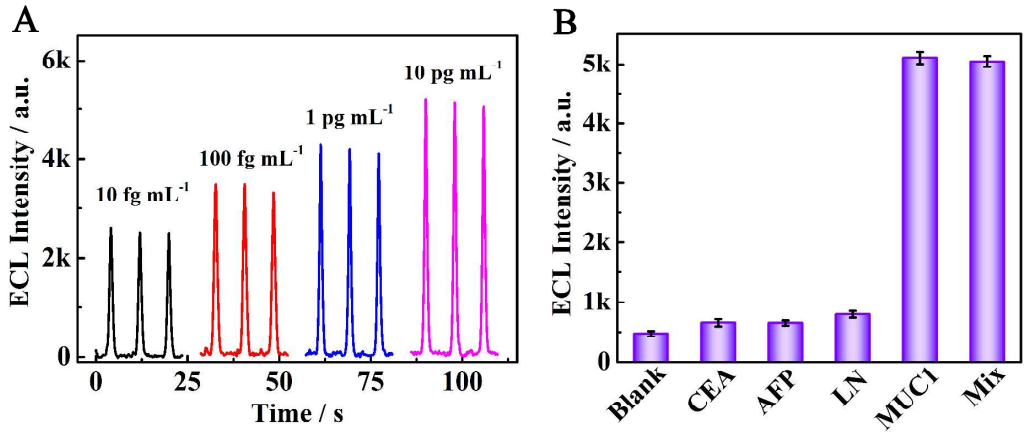

Figure 5. (A) The stability of the prepared biosensor under various concentrations of MUC1. (B) The specificity of the proposed biosensor toward different interfering

substances.

Application of the biosensor in human serum. To evaluate the applicability of the proposed biosensor, we challenged our sensor for determination MUC1 in a complicated sample matrix by dispensing different concentrations of target MUC1 with human serum (supported by Xinqiao Hospital, 50-fold-diluted before use) via a standard addition method. As shown in Table 4, to every added target concentration, we calculated a "found concentration" according to the above obtained linear regression equation. Thus, the recovery (the ratio between the found concentration and added concentration) were calculated to be 99.57%, 90.60%, 98.08% and 96.02%, respectively with a satisfactory RSD from 2.78% to 5.56%. The results indicated that the proposed biosensor had a potential application in clinical determination of MUC1.

Table 4. Detection MUC1 in human serum (n = 3) for recovery study.

Added MUC1 concentration / pg mL^{-1}	Concentration found / pg mL^{-1}	Recovery / %	RSD / %
0.100	0.09957	99.57	2.91%
1.00	0.9060	90.60	2.78%
10.0	9.808	98.08	5.56%
100	96.02	96.02	3.35%

CONCLUSIONS

In summary, a novel ECL biosensor was fabricated based on an effective 3-D DNA nanomachine signal probe induced by protein-aptamer binding complex which realized the direct recycling of protein in the fabrication of biosensor without protein conversion for ultrasensitive detection of MUC1. The higher sensitivity and lower detection limit of the proposed biosensor should be ascribed to the following reasons.

Firstly, the 3-D DNA nanomachine signal probe was assembled in a solution environment, which allowed the CHA to react unencumberedly in all directions leading to large amounts of luminophore ABEI be immobilized on $CoFe_2O_4$ surface with higher ECL signal. Secondly, $CoFe_2O_4$ was used as the nanocarrier of the 3-D DNA nanomachine signal probe to catalyze the decomposition of co-reactant H_2O_2 to produce abundant $OH^{\cdot}$, an essential intermediate for ABEI ECL reaction. Thirdly, the cyclic reuse of MUC1-aptamer was also devoted to the excellent sensitivity of the biosensor without protein conversion and enzyme introduction. Hence, this method may provide a convenient, economic and effective strategy for biomolecules sensitive detection in clinical analysis, especially for trace proteins in the early stage of cancer.

AUTHOR INFORMATION

* Corresponding authors:

Tel.: +86-23-68252277; Fax: +86-23-68253172.

E-mail address: yuanruo@swu.edu.cn (R. Yuan), yqchai@swu.edu.cn (Y. Q. Chai)

ACKNOWLEDGEMENTS

This work was financially supported by the NNSF of China (21675129, 51473136, 21575116), the China Postdoctoral Science Foundation (2016M602626), and the Fundamental Research Funds for the Central Universities (XDJK2015A002), China.

REFERENCES

(1) Chikkaveeraiah, B. V.; Bhirde, A. A.; Morgan, N. Y.; Eden, H. S.; Chen, X.Y. *ACS nano*, **2012**, *6*, 6546-6561.

(2) Chinen, A. B.; Guan, C. M.; Ferrer, J. R.; Barnaby, S. N.; Merkel, T. J.; Mirkin, C. A. *Chem. Rev.*, **2015**, *115*, 10530-10574.

(3) Fu, C. L.; Liu, C.; Li, Y.; Guo, Y. J.; Luo, F.; Wang, P. L.; Guo, L. H.; Qiu, B.; Lin,

Z. Y. *Anal. Chem.*, **2016**, *88*, 10176-10182.

(4) Graybill, R. M.; Bailey, R. C. *Anal. Chem.*, **2016**, *88*,, 431-450.

(5) Yang, Z. H.; Zhuo, Y.; Yuan, R.; Chai, Y. Q. *Anal. Chem.*, **2016**, *88*, 5189-5196.

(6) Fredriksson, S.; Gullberg, M.; Jarvius, J.; Olsson, C.; Pietras, K.; Gústafsdóttir, S. M.; Osman, A.; Landegren, U. *Nat. Biotechnol.*, **2002**, *20*, 473-477.

(7) Tan, Y.; Wei, X. F., Zhang, Y.; Wang, P. L.; Qiu, B.; Guo, L. H.; Lin, Z. Y.; Yang, H. H. *Anal. Chem.*, **2015**, *87*, 11826-11831.

(8) Huang, Y.; Liu, X. Q.; Huang, H. K.; Qin, J.; Zhang, L. L.; Zhao, S. L., Chen, Z. F.; Liang, H. *Anal. Chem.*, **2015**, *87*, 8107-8114.

(9) You, M. X.; Chen, Y.; Zhang, X. B.; Liu, H. P., Wang, R. W.; Wang, K. L.; Williams, K. R.; Tan, W. H. *Angew. Chem., Int. Ed.,* **2012**, *124*, 2507-2510.

(10) Yang, Y. Y.; Goetzfried, M. A.; Hidaka, K.; You, M. X.; Tan, W. H.; Sugiyama, H.; Endo, M. *Nano Lett.*, **2015**, *15*, 6672-6676.

(11) Zhou, C.; Duan, X. Y.; Liu, N. *Nat. Commun.*, **2015**, *6*, 8102.

(12) Cha, T. G.; Pan, J.; Chen, H. R.; Salgado, J.; Li, X.; Mao, C. D.; Choi, J. H. *Nat. Nanotechnol.*, **2014**, *9*, 39-43.

(13) Wickham, S. F. J.; Bath, J.; Katsuda, Y.; Endo, M.; Hidaka, K.; Sugiyama, H.; Turberfield, A. J. *Nat. Nanotechnol.*, **2012**, *7*, 169-173.

(14) Liber, M.; Tomov, T. E.; Tsukanov, R.; Berger, Y.; Nir, E. *Small*, **2015**, *11*, 568-575.

(15) Liu, M. H.; Fu, J. L.; Hejesen, C.; Yang, Y. H.; Woodbury, N. W.; Gothelf, K.; Yan, L.; Yan, H. *Nat. Commun.*, **2013**, *4*, 2127.

(16) Zhou, C.; Yang, Z. Q.; Liu, D. S. *J. Am. Chem. Soc.*, **2012**, *134*, 1416-1418.

(17) Zhang, H. Q.; Lai, M. D.; Zuehlke, A.; Peng, H. Y.; Li, X. F.; Le, X. C. *Angew. Chem.*, **2015**, *127*, 14534-14538.

(18) Yang, X. L.; Tang, Y. N.; Mason, S. D.; Chen, J. B.; Li, F. *ACS nano*, **2016**, *10*, 2324-2330.

(19) Yin, P.; Choi, H. M.; Calvert, C. R.; Pierce, N. A. *Nature*, **2008**, *451*, 318-322.

(20) Wu, C. C.; Cansiz, S.; Zhang, L. Q.; Teng, I. T.; Qiu, L. P.; Li, J.; Liu, Y.; Zhou, C. S.; Hu, R.; Zhang, T.; Cui, C.; Cui, L.; Tan, W. H. J. Am. Chem. Soc., **2015**, *137*, 4900-4903.

(21) Li, J. N.; Liu, W. Q.; Wu, X. C.; Gao, X. F. *Biomaterials*, **2015**, *48*, 37-44.

(22) Xia, X. H.; Zhang, J. T.; Lu, N.; Kim, M. J.; Ghale, K.; Xu, Y.; Mckenzie, E.; Liu, J. B.; Ye, H. H. *ACS Nano*, **2015**, *9*, 9994-10004.

(23) Chen, Z. W.; Yin, J. J.; Zhou, Y. T.; Zhang, Y.; Song, L.; Song, M. J.; Hu, S. L.; Gu, N. *ACS Nano*, **2012**, *6*, 4001-4012.

(24) Andre, R.; Natalio, F.; Humanes, M.; Leppin, J.; Heinze, K.; Wever, R.; Schroder, H. C.; Muller, W. E. G.; Tremel, W. *Adv. Funct. Mater.*, **2011**, *21*, 501-509.

(25) Shi, W. B.; Zhang, X. D.; He, S. H.; Huang, Y. M. *Chem. Commun.*, **2011**, *47*, 10785-10787.

(26) Sun, Y. G.; Xia, Y. N. *Science*, **2002**, *298*, 2176-2179.

(27) He, Y.; Wang, Y.; Yang, X.; Xie, S. B.; Yuan, R.; Chai, Y. Q. *ACS Appl. Mater. Interfaces*, **2016**, *8*, 7683-7690.

(28) Cheng, A. K. H.; Su, H. P.; Wang, Y. A.; Yu, H. Z. *Anal. Chem.*, **2009**, *81*, 6130-6139.

(29) Deng, C. Y.; Pi, X. M.; Qian, P.; Chen, X. Q.; Wu, W. M.; Xiang, J. *Anal. Chem.*, **2017**, *89*, 966-973.

(30) Jiang, X. Y.; Wang, H. J.; Wang, H. J.; Yuan, R.; Chai, Y. Q. *Anal. Chem.*, **2016**, *88*, 9243-9250.

For TOC Only

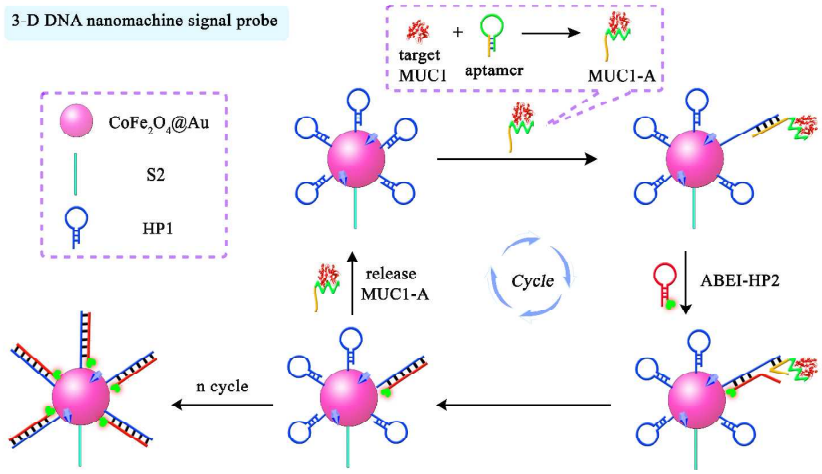
3-D DNA nanomachine signal probe
target MUC1
aptamer
MUC1-A
CoFe2O4@Au
S2
HP1
release MUC1-A
Cycle
ABEI-HP2
n cycle